ADVANCED FUNCTIONAL MATERIALS
www.afm-journal.de

Extracellular Matrix Control of Collagen Mineralization In Vitro

*Alexander J. Lausch, Bryan D. Quan, Jason W. Miklas, and Eli D. Sone**

Collagen biomineralization is a complex process and the controlling factors at the molecular level are still not well understood. A particularly high level of spatial control over collagen mineralization is evident in the anchorage of teeth to the jawbone by the periodontal ligament. Here, unmineralized ligament collagen fibrils become mineralized at an extremely sharp mineralization front in the root of the tooth. A model of collagen biomineralization based on demineralized cryosections of mouse molars in the bone socket is presented. When exposed to metastable calcium and phosphate-containing solutions, mineral re-deposits selectively into the natively mineralized tissues with high fidelity, demonstrating that the extracellular matrix retains sufficient information to control the rate of mineralization at the tissue level. While solutions of simulated bodily fluid produce amorphous calcium phosphate within the tissue section, a more highly supersaturated solution stabilized with polyaspartic acid produces oriented, crystalline calcium phosphate with diffraction patterns consistent with hydroxyapatite. The model thus replicates both spatial control of mineral deposition, as well as the matrix-mineral relationships of natively mineralized collagen fibrils, and can be used to elucidate roles of specific biomolecules in the highly controlled process of collagen biomineralization. This knowledge will be critical in the design of collagen-based scaffolds for tissue engineering of hard-soft tissue interfaces.

1. Introduction

The mineralized collagen fibril is a complex composite structure that forms the basis of mineralized connective tissues, such as bone, cementum, and dentin.[1] The crystalline mineral phase of mature tissues, hydroxyapatite (HA), is first found in the gap zones of the collagen fibril,[2,3] with the c-axis of the HA crystals parallel to the long axis of the collagen fibril.[4,5] The intricate organization of these inorganic and organic components, and the complex interactions between them, are critical to the properties of such mineralized connective tissues.[6] Although it is widely accepted that extracellular matrix macromolecules,[7] and particularly acidic, phosphorylated non-collagenous proteins (NCPs),[8] can affect many aspects of HA nucleation and growth, the precise mechanistic details of collagen mineralization have not yet been satisfactorily resolved. Fundamental questions remain, including the question of what controls whether or not collagen in different tissues is mineralized. Understanding the molecular factors that control collagen mineralization will be critical for the development of collagen-based scaffolds for tissue engineering of hard-soft interfaces, such as in ligament and tendon attachment.

Biological collagen mineralization is a dynamic process, involving a complex interplay between cells, secreted macromolecules, signalling molecules, and enzymatic reactions.[7] Given this complexity, several model systems have been developed with which to study the role of collagen itself and various extracellular matrix macromolecules in the mineralization process. The evidence these models provide, however, is sometimes contradictory. For example, in an in vitro agarose gel model, one phosphorylated NCP (dentin phosphophoryn, DPP), showed promotion of HA formation at low concentrations, but inhibition at high concentrations.[9] Furthermore, DPP has been shown to promote HA formation when immobilized to collagen,[10,11] but inhibits its formation in solution.[8,12] To better understand the factors affecting mineralization, collagen-based models that replicate the native environment are needed.

A critical measure of the success of a model of collagen mineralization is its ability to replicate the process of mineralization, as well as the composite structure of the naturally mineralized collagen fibril, with respect to mineral phase, morphology, alignment, and spatial distribution. A recent breakthrough in this regard was achieved by Gower and co-workers, who mineralized reconstituted type-I collagen scaffolds using a supersaturated calcium and phosphate-containing solution stabilized by polyaspartic acid (polyAsp).[13] This system not only resulted in oriented HA crystals within collagen fibrils, but mineralization proceeded through an initial amorphous calcium phosphate (ACP) precursor, for which there is growing in vivo evidence.[14] Although the precise role of polyAsp is still the subject of debate, it and other stabilizing macromolecules have since been used to mineralize reconstituted collagen fibrils directly on transmission electron microscopy (TEM) grids[15–17] as well as in demineralized tissues.[18,19] Wang et al. recently showed

A. J. Lausch, B. D. Quan, J. W. Miklas,
Prof. E. D. Sone
Institute of Biomaterials & Biomedical Engineering
Department of Materials Science & Engineering
and Faculty of Dentistry
University of Toronto
Toronto, ON M5S 3G9, Canada
E-mail: eli.sone@utoronto.ca

DOI: 10.1002/adfm.201203760

that it is possible to achieve oriented HA in a dense collagen scaffold without soluble additives, also through an amorphous precursor, albeit using a mineralizing solution with very high supersaturation.[20] Despite these significant advancements, a limitation of many of these models is the use of reconstituted collagen as the mineralization substrate, which lacks natural fibrillar packing and cross-linking seen in native tissues, along with collagen-bound macromolecules.

Several natural tissues have been used as substrates for in vitro collagen mineralization models, including turkey leg tendon,[18,21] rat tail tendon,[19] demineralized bone,[19,22–24] and periodontal ligament.[25] These models, however, do not offer a direct comparison between unmineralized and mineralized tissues. In the periodontium, the set of connective tissues involved in anchoring the tooth root to the jawbone, the juxtaposition of mineralized and non-mineralized collagenous tissues presents an excellent model with which to study molecular factors controlling collagen mineralization. In particular, the attachment of the periodontal ligament (PDL) to the root involves a highly controlled process in which bundles of ligament fibrils become embedded in the outer mineralized layer of the tooth root (cementum) at an extremely well-defined mineralization front.[26] We present here a model of collagen biomineralization based on demineralized tissue sections of mouse molars. By exposing these sections to metastable mineralizing solutions, we demonstrate that the extracellular matrix in the demineralized section retains sufficient information to direct preferential remineralization of the natively mineralized tissues.

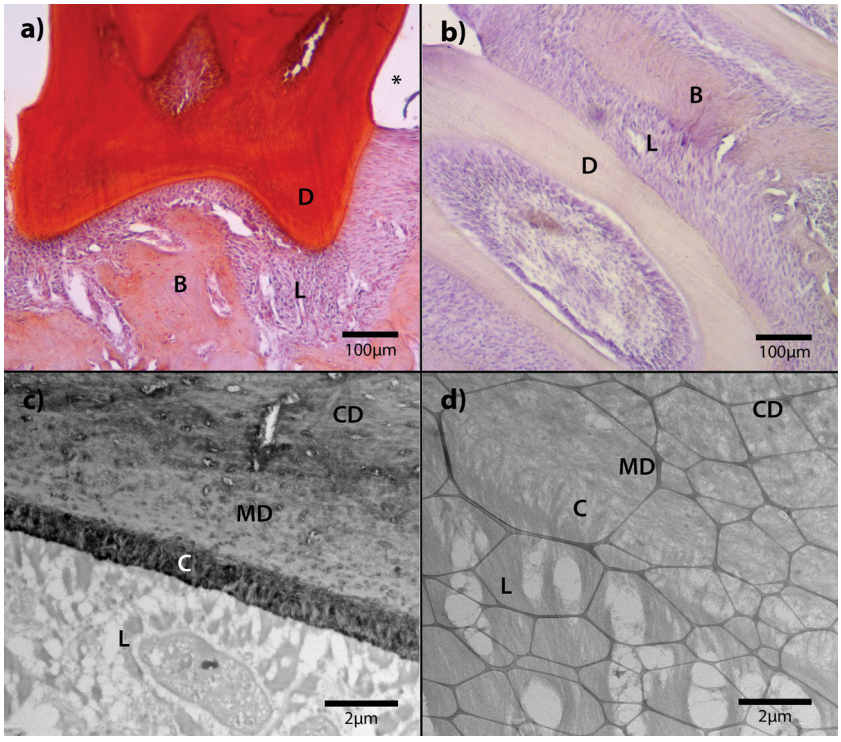

Figure 1. Fixed, demineralized mouse molars in the supporting bone socket, remineralized in m-SBF shown in a,b) light and c,d) electron microscopy. a) 5-µm-thick section stained with Alizarin Red after one day of mineralization. The asterisk indicates the glass slide. b) Control section stained with Alizarin Red following two-step demineralization in EDTA. Pink colour is an artifact due to slight collagen counter-staining. c) Ultrathin (210 nm) section remineralized in m-SBF for 13 days imaged in TEM. Increased electron density is indicative of mineral content, as the section is unstained. d) Control section following demineralization, in which no mineral is apparent. The porous pattern visible is the lacey carbon support of the TEM grid. (D–dentin, B–bone, C–cementum, CD–circumpulpal dentin, MD–mantle dentin, L–ligament).

2. Results

To examine the role of the extracellular matrix (containing both collagen and fixed non-collagenous proteins) in the control of mineralization in the periodontium, we exposed demineralized periodontal tissue sections from mouse molars to metastable calcium and phosphate-containing solutions. **Figure 1**a shows 5 µm thick cryosections that were remineralized for one day in modified simulated body fluid (m-SBF),[27] following demineralization in ethylenediaminetetraacetic acid (EDTA) (Figure 1b), and stained with Alizarin Red. Only the tissue section itself is mineralized; no mineral was seen on the glass slide, and no precipitate was observed in the solution. Selective remineralization within the section is characterized by preferential mineralization of hard connective tissues (dentin and bone), while the soft periodontal ligament (PDL), remains largely unmineralized at this time point. We note that at longer mineralization time points the PDL does begin to mineralize (not shown), that control over mineralization is not absolute, but rather the relative rate of mineralization is different among the various tissues. Dentin evidently mineralizes more rapidly than bone, as it is more intensely stained. We focused on the PDL-cementum junction in ultra-thin sections (Figure 1c), in which after 13 days in m-SBF, dentin and particularly cementum show greater electron density indicative of mineral deposition, while the PDL remains unmineralized. We note that the overall rate of mineralization in thin sections was significantly slower than for thick sections, as the mineralization solution was not stirred. The interface between cementum and PDL is finely controlled, with a very sharp mineralization front similar to the native tissue.[26] Within the dentin, circumpulpal dentin and mantle dentin can be distinguished, presumably due to differences in collagen fibril orientation.[28] Figure 1d shows the same tissue area in a control section, in which no evidence of mineral was found in any tissue following two demineralization steps. These results show that the extracellular matrix of demineralized tissue can control the rate of mineral deposition from a purely inorganic solution.

A detailed examination of remineralized dentin from m-SBF solution (two days, **Figure 2**) revealed specific collagen-mineral relationships. At intermediate magnification (Figure 2a), the directionality of the collagen fibrils is clearly

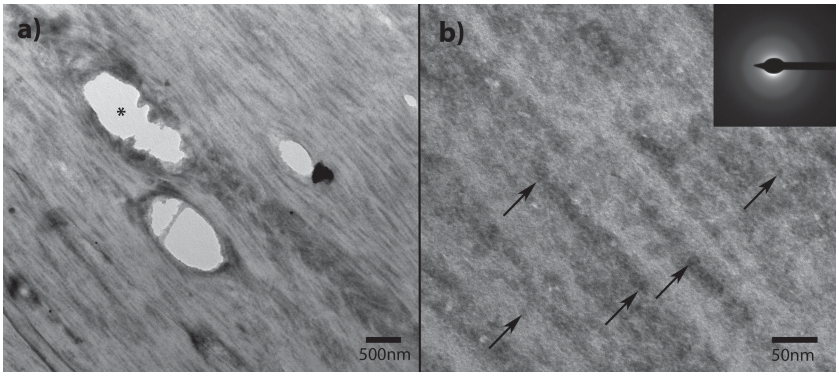

Figure 2. TEM images of mouse dentin after remineralization in m-SBF for 3 days. a) Orientation of collagen fibrils is readily apparent, as are individual collagen fibrils more electron dense than the surrounding tissue. An asterisk indicates a dentin tubule. Note increased density of mineral in some regions of peritubular dentin. b) Higher magnification showing globular mineral deposits (arrows) along collagen fibrils. Inset shows an electron diffraction pattern with only a very diffuse ring, indicating that the mineral is amorphous.

evident, and individual collagen fibrils can be resolved as dark lines suggesting that the fibrils themselves are mineralized. We note that certain groups of fibrils are more heavily mineralized than others, as are some regions of peritubular dentin. In higher magnification images (Figure 2b), collagen fibrils are still apparent (≈80 nm in diameter), and the mineral morphology can be seen to be globular, with clusters ranging in size from 5–10 nm, suggestive of an amorphous phase. Indeed, electron diffraction (Figure 2b, inset) produced a single diffuse diffraction ring. Radial integration (not shown) showed the diffuse ring to be centered at a d-spacing of 3.18 Å, which is close to values reported for biological amorphous calcium phosphate (ACP).[14] At longer time points (13 days), the mineral was still amorphous, and was found to have a Ca/P ratio 1.03 ± 0.08 by energy dispersive X-ray analysis (EDX). These results show that the mineral is ACP. We note that the same phase was found in cementum and bone in the remineralized sections. This ACP phase is apparently very stable, and does not transform under the electron beam, or after several months following removal of the sections from solution.

The presence of acidic polymers such as polyaspartic acid (polyAsp) in the mineralizing solution, ostensibly as a substitute for soluble non-collagenous proteins, has been shown to produce intrafibrillar crystalline mineral in other models of collagen mineralization.[15,16,18,22] We therefore tested whether the addition of polyAsp to m-SBF affects the mineral phase formed in demineralized periodontal tissues. **Figure 3** shows sections remineralized for 13 days in m-SBF with and without polyAsp (125 μm/mL). The addition of polyAsp slowed the rate of mineral deposition, but did not change the mineral phase. Electron diffraction patterns still showed only a diffuse ring, regardless of the presence of polyAsp (Figure 3b inset). Interestingly, EDX showed a significantly higher Ca/P ratio (1.46 ± 0.09) for mineral formed from the polyAsp-containing solution.

Magnesium and carbonate ions, both of which are present in significant concentrations in m-SBF, have both been shown to inhibit ACP to HA transformations by reducing ACP solubility.[29,30] We therefore explored alternative mineralizing solutions. Beniash and co-workers have shown that high phosphate mineralizing solutions (CaP1, **Table 1**), which are unstable on their own, can be stabilized with the addition of polyAsp and used to produce intrafibrillar crystalline mineral in reconstituted collagen fibrils.[15] Demineralized periodontal tissue sections remineralized with CaP1 solutions containing 62.5 μg/mL polyAsp also demonstrated spatial selectivity in mineral deposition (**Figure 4**). As with m-SBF solutions, the PDL initially remained unmineralized, at a time point at which all natively mineralized tissues remineralized. Circumpulpal dentin, mantle dentin and cementum all appear to have similar mineral content at 2 h. Sharpey's fibres, collagen fibres that traverse the PDL-cementum junction, become mineralized along a sharp mineralization front, similar to native tissue. We note that increasing the concentration of polyAsp slowed the overall rate of mineralization, but had no other evident effect. In contrast with m-SBF-mineralized sections, electron diffraction patterns of all three mineralized tissues, showed crystalline, oriented diffraction patterns (**Figure 5**), very similar to what is obtained from native mineralized connective tissues. Arcs with a d-spacing of 3.52 Å, consistent with the (002) plane of hydroxyapatite (HA, JCPDS# 9-432), showed preferential orientation along the long axis of the collagen fibrils. A more diffuse ring, with a d-spacing of 2.87 Å, corresponds to the closely spaced (211), (112), and (300) planes. Ca/P ratios obtained by EDX for dentin mineralized with CaP1 solutions for 8 h were shown to be on average 1.40 ± 0.03. This Ca/P ratio is lower than typical for HA, and may be due to organic phosphate in the tissue, or the presence of more than one phase. We

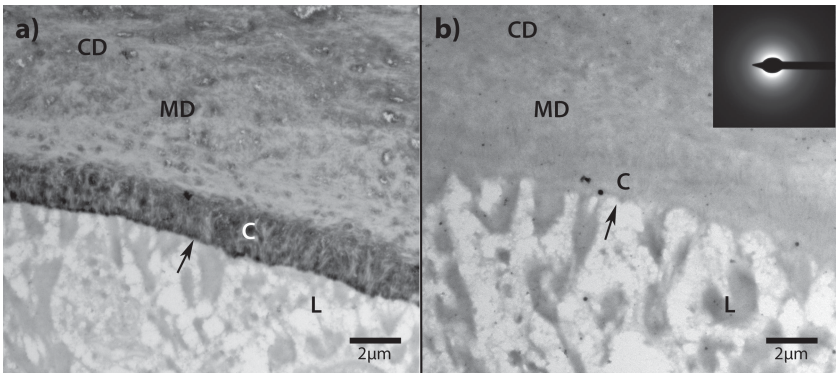

Figure 3. TEM images comparing remineralization, for 13d, using m-SBF a) without and b) with polyaspartic acid (125 μg/mL). It is clear that polyAsp slows mineralization, however selectivity is not affected. The arrows indicated the cementum-PDL junction. The inset of Figure 3b shows electron diffraction from dentin remineralized with m-SBF containing 125 μg/mL polyAsp for 13 days, indicating the mineral remains amorphous. (D–dentin, B–bone, C–cementum, CD–circumpulpal dentin, MD–mantle dentin)

Table 1. Ion concentrations of mineralizing solutions in mM. CaP solutions are stabilized with 62.5–125 μg/mL polyAsp.

Solution	$[Na^+]$	$[K^+]$	$[Mg^{2+}]$	$[Ca^{2+}]$	$[Cl^-]$	$[HCO_3^-]$	$[P_i]^{a)}$	$[SO_4^{2-}]$	$logS_{HA}^{b)}$
m-SBF [26]	142	5	1.5	2.5	103	10	1.0	0.5	9.9
CaP1 [15]	133	3.5	0	1.7	123	0	9.1	0	11.6
CaP2	104	0	0	9.1	110	0	1.7	0	13.3
CaP3 [13]	154	0	0	4.5	163	0	2.1	0	11.9

[a)]Total inorganic phosphate concentration; [b)]Log of supersaturation ratio (S) with respect to hydroxyapatite ($S=IP/K_{sp}$ where IP is the ion activity). Calculations were performed in Visual Minteq (KTH Royal Institute of Technology, Sweden).

note that in the absence of polyAsp, the CaP1 remineralizing solution rapidly precipitates on its own, and control remineralization experiments in such solutions resulted in random distribution of HA on the surface of the tissue section (not shown).

A detailed examination of the dentin remineralized in CaP1 solution with polyAsp reveals specific matrix-mineral relationships. **Figure 6** shows a section mineralized for 2 h, in which individual collagen fibrils, somewhat more electron dense than the interfibrillar space, are apparent. A faint banding pattern of alternating dark and light bands can be seen in most of the fibrils. The darker bands are presumably more electron dense due to the presence of mineral, as the sections are unstained. These bands occupy a length of 34 ± 5 nm on average along the long axis of the fibril, which is close to the collagen gap region dimension of ≈40 nm. In some regions, the mineral occupying the bands appears diffuse, without distinct features, while in other regions distinct dark striations (7–9 nm in width), aligned with the long axis of the collagen fibril, are observed. Some of these striations, which we interpret as individual crystallites or groups of crystals, are confined within a single band (e.g., left selected area in Figure 6). In other cases they are longer (30–60 nm), and not restricted to a single band (e.g., right enlargement in Figure 6). The more diffuse regions may indicate the presence of ACP, or may be due to a different orientation of plate-shaped crystallites. In any case, the pattern of mineralization, consisting of oriented crystallites, sometimes with axial periodicity along the collagen fibrils, is remarkably reminiscent of the pattern seen in early mineralizing bone (e.g., embryonic chick bone[31]) and mineralizing turkey tendon.[4]

We tested different variations on the CaP1 solution, all containing 125 μg/mL polyAsp, (Table 1) to determine the factors that govern the formation of ACP vs. HA in our model system. A remineralizing solution with calcium and phosphate concentrations reversed relative to the original (CaP2) produced only ACP (not shown). Likewise, solutions similar to those used by Olszta et al.[13] (CaP3, which contains higher calcium concentration but similar supersaturation to CaP1), also produced only ACP within the tissue sections (not shown). We note that Olszta et al. did obtain crystalline mineral was with this solution using reconstituted collagen, albeit with a lower concentration of polyAsp. Notably, in all these alternate solutions the overall rate of mineralization was significantly slower than for CaP1, even when the supersaturation with respect to HA was the same or higher. Thus, in our model system, a mineralizing solution containing high phosphate concentration was necessary to produce HA.

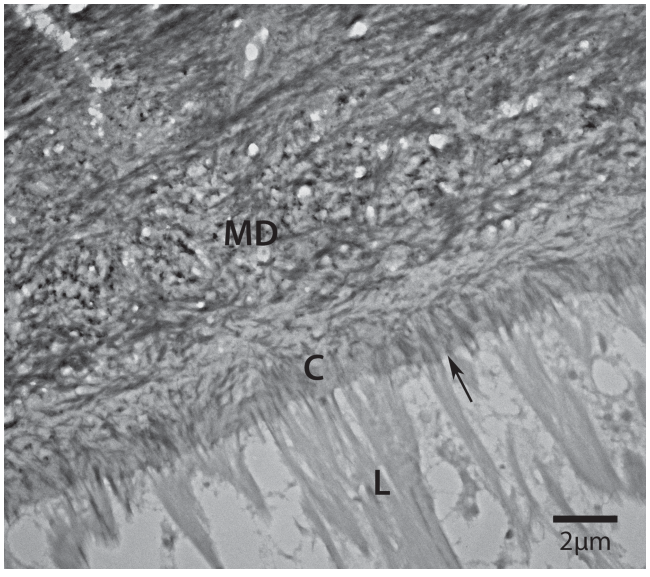

Figure 4. TEM image of tissue remineralized in CaP1 solution with 62.5 μg/mL polyAsp for 2 h. Dentin and cementum are mineralized, whereas the PDL remains unmineralized. The sharp mineralization front, at the cementum/PDL junction, is indicated by the arrow. (C–cementum, CD–circumpulpal dentin, MD–mantle dentin])

3. Discussion

Using a tissue-based model of collagen mineralization, we demonstrate that the fixed, demineralized extracellular matrix (ECM) of mouse dental and periodontal tissues retains sufficient molecular memory to direct selective remineralization from metastable calcium and phosphate-containing solutions. The natively mineralized tissues (dentin, cementum and bone) remineralize preferentially over the periodontal ligament, with high level of spatial control, similar to what is observed in vivo. In remineralization solutions of m-SBF, the mineral formed as globular particles of ACP associated with collagen fibrils. In more highly supersaturated solutions (CaP1), stabilized by polyAsp, c-axis oriented, crystalline HA was formed with axial periodicity along collagen fibrils, similar to native mineralized collagen. Together, these results suggest that while the ECM alone can guide rate of mineralization in different tissues, the presence of a soluble additive (polyAsp) was necessary to replicate the HA-collagen composite structure in mineralized connective tissues.

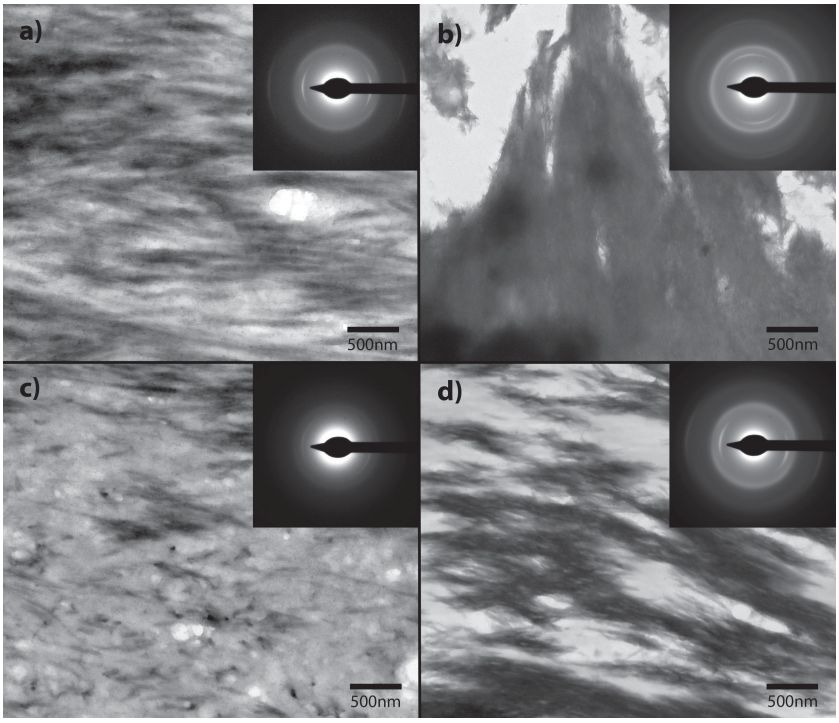

Figure 5. TEM images show a) circumpulpal dentin, b) cementum, c) mantle dentin, and d) bone remineralized in CaP1 solution (125μg/mL polyAsp) for 2 (a,c), 5 (d) and 11 (b) h. Insets show diffraction patterns corresponding to oriented, crystalline mineral in all tissues. The time point for each tissue was chosen based on the presence of sufficient mineral to produce a clear diffraction pattern.

While several researchers have examined in vitro mineralization of tissues, our model is unique in that it contains the finely juxtaposed hard and soft tissues of the periodontium. In principle, this internal control can be used to investigate the molecular factors that control mineralization of collagenous tissues, both as part of the ECM and in solution. Differences in rates of mineral deposition into the mineralized tissues themselves may be instructive in this respect as well. By working with thin cryo-sections, we minimize diffusion effects that may complicate mineralization of bulk tissues, and maintain the tissue in a hydrated state throughout the processing. Simultaneous fixation and demineralization of the tissue ensures a high degree of preservation, retaining collagen structure and insoluble macromolecular content.[32] While we attempted to preserve the native tissue structure insofar as possible, the processing steps necessarily alter the tissue to some extent. Despite simultaneous fixation, the demineralization removes some soluble (i.e., non matrix-bound) and mineral bound proteins, for instance, while fixation itself can alter protein conformation. Moreover, the fixed tissue model ignores the complex and dynamic cellular and enzymatic processes that occur during mineralization in vivo. Nevertheless, it is remarkable that despite these limitations, such a high level of spatial control over mineral deposition is maintained, even in simple inorganic solutions such as m-SBF.

The ECM alone can control the rate of mineral deposition, but in purely inorganic solutions (e.g., m-SBF), did not lead to the formation of crystalline mineral. Only relatively highly supersaturated solutions containing high phosphate concentrations and incorporating polyAsp, such as those prepared by Deshpande et al. (CaP1 solution),[15] resulted in the formation of apatitic mineral. The mineralization pattern from these solutions mimics the early mineralization of collagen in connective tissues both in crystal size and distribution within collagen fibrils. Such solutions were shown previously to form oriented HA within reconstituted collagen through an ACP intermediate, although lacking in axial periodicity. Likewise, polyAsp-containing solutions with similar supersaturation but lower phosphate content have been used to remineralize tissues,[18,19] and reconstituted collagen[13,16,33] through an ACP to HA transformation, and recent work has shown that other stabilizing additives can produce similar results.[16,17] In our model, only the high phosphate solution led to crystalline mineral. This solution also had the highest rate of mineralization, which we suggest leads to the formation of less stable ACP, and which is therefore more readily converted to HA. The dependence of the stability of ACP on its rate of formation has been described previously,[34] and was explained by increased incorporation of foreign ions and smaller cluster size for rapidly formed ACP, leading

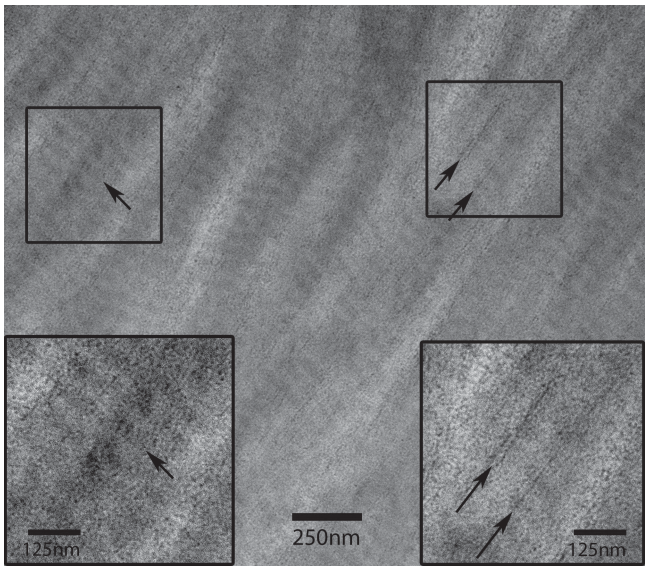

Figure 6. TEM image of dentin remineralized in CaP1 solution (125 μg/mL polyAsp) for 2 h. Individual collagen fibrils showing alternating light and dark bands are visible. The bottom left image is an enlargement of the selected area above. Dark striations, corresponding to individual crystallites or groups, are visible. The small arrows on the left side indicate areas in which these crystallites are restricted to the dark bands of the fibril. The bottom right image is an enlargement of the selected area above, showing a region in which the dark striations are not restricted to a single band.

to higher solubility. In a similar vein, Meyer and Eanes have shown that lower Ca/P ratios in solution resulted in smaller induction times of the crystalline transformation of ACP.[35] The relatively low Ca/P ratio (1.40 ± 0.03) of the mineral formed in the tissue sections is also consistent with the presence of ACP, as is the presence of some diffuse mineral (Figure 6). We note that the presence of octacalcium phosphate (OCP)[35,36] would also lower the Ca/P ratio. Although we cannot rule out this possibility, we found no evidence of the larger, more well-developed crystals typical of OCP.[37] Taken together, these data suggest that in our model, mineralization also follows an ACP to HA transition, and that the rate of precipitation within the tissue determines induction time for this transition.

We suggest that rate of ACP formation governs its stability in our model system. A question remains, however, as to why the high phosphate solution had the highest rate of mineralization, especially since lower Ca/P ratios would normally be expected to slow precipitation from solution.[38] Apparently, in our model, the concentration of calcium ions has much less of an effect than concentration of phosphate on the rate of tissue mineralization. This suggests that the tissue is probably saturated with respect to bound Ca^{2+} in all solutions, and the amount of polyAsp-bound or free Ca^{2+} is less important for nucleation within the section. Solutions with higher free phosphate concentrations can thus produce greater local supersaturations in the tissue, and thus a higher rate of heterogeneous nucleation. The more rapidly formed ACP is less stable, and transforms to HA, as discussed above. Although the phosphate concentration of CaP1 is significantly higher than blood serum, the ionic composition at the mineralization front may be quite different from the bulk bodily fluid, due to dynamic processes. It has been recently suggested in this regard that enzymatic breakdown of polyphosphates at the mineralization front produces high local concentrations of inorganic phosphate, for instance.[39]

Regardless of the mineral phase formed, in all solutions the rate of mineralization was drastically different between mineralized and non-mineralized tissues, leading to a pattern of mineralization that mimics native periodontium. Furthermore, the difference in mineralization rates was not exclusive to unmineralized tissues. We observed preferential mineralization of dentin and cementum over bone in all solutions, as well as preferential mineralization of peritubular dentin over intertubular dentin. While it is clear that the ECM is controlling the rate of mineralization, it is intriguing to speculate about which specific ECM macromolecules lead to these differences. Certainly collagen type, post-translational modification, and cross-linking, are known to be tissue specific,[40,41] and have been suggested to affect its susceptibility to mineralization.[42] But differences in the distribution of non-collagenous macromolecules are most dramatic, particularly with respect to the acidic non-collagenous proteins of mineralized tissues,[8] and well known differences in proteoglycan content between mineralized and non-mineralized tissues,[43] which may promote or inhibit mineralization in these tissue types. Within the natively mineralized tissues, the higher rate of mineralization of dentin as compared to bone is consistent with the high amount of dentin sialoprotein (DSP, thought to be a promoter) in dentin, and greater amounts of osteopontin (OPN, thought to be an inhibitor) in bone.[44] Likewise peritubular dentin, which is preferentially mineralized in our model has a particularly high concentration of acidic non-collagenous phosphoproteins.[45] The case of cementum confounds the issue somewhat, as it mineralized preferentially to dentin only in m-SBF, which indicates that there is some level of rate-dependence due to soluble molecules–not solely ECM. Nevertheless, the influence of the ECM is remarkable. Perhaps the greatest strength of this model is that it can in principle be used to probe the different factors involved in control of mineralization, both at the tissue level and at the fibrillar level, either through changing solution composition or selective digestion of certain ECM components.

4. Conclusions

Our tissue section-based model of collagen mineralization shows that ECM macromolecules can control the rate of mineral deposition from metastable mineralizing solutions into fixed, demineralized tissues, such that the native pattern of mineralization is recreated with high fidelity. This control is not specific to a particular mineralizing solution composition, and does not require the addition of any organic component to the solution. The ECM alone was not sufficient, however, to guide mineral phase. Only solutions with relatively high phosphate concentration, stabilized with polyAsp, produced crystalline, oriented mineral within the mineralized tissues, mimicking the mineral-matrix relationship of mineralized connective tissues. This model can be employed to elucidate the roles of specific macromolecules in inhibiting and/or promoting mineralization in collagenous tissues.

5. Experimental Section

Unless otherwise noted, all reagents were obtained from Sigma-Aldrich (Oakville, ON, Canada) and MilliQ-filtered water was used. Animal protocols were approved by the Animal Care Committee at the University of Toronto and conducted according to their guidelines.

Tissue Processing: Five week old CD1 mice (Charles River, QC, Canada) were sacrificed by cervical dislocation. Their mandibles were excised, separated into hemimandibles and extraneous soft tissue was removed. The clean hemimandibles were fixed in 0.8% paraformaldehyde (Electron Microscopy Sciences, PA, USA) and 0.2% glutaraldehyde (Canemco, QC, Canada) in Dubecco's PBS (Invitrogen, USA) at pH 7.4 for 24 h (glutaraldehyde was not used in tissue preparation for thick sections). The hemimandibles were demineralized in 0.2% paraformaldehyde, 0.05% glutaraldehyde and 9.5% EDTA for 7 days (pH 7.4) at 4 °C with rocking. Demineralizing solution was changed daily.

Ultrathin Sectioning and Second Demineralization (for TEM): Following demineralization, hemimandibles were infiltrated with several changes of 2.3 M sucrose solution for cryoprotection and stored in fresh sucrose at 4 °C. The tissue was trimmed to isolate the 3 molars in the bone socket and frozen in sucrose on a mounting pin at –80 °C. First molars were sectioned, through the transverse plane, on a Leica EM UC6-NT ultracryomicrotome at –90 °C using a cryo-immuno diamond knife (DiATOME, CH). 210-nm thin sections were transferred to 200 mesh, lacy carbon supported, nickel grids (Electron Microscopy Sciences) and floated on 2 changes of water to remove sucrose. The grids were then floated on drops of 12.5% EDTA to ensure complete demineralization. After 24 h the grids were floated on a stirred water bath for 30 min before remineralization to remove residual EDTA, followed by two exchanges in fresh water.

Thick Sectioning and Second Demineralization (for LM): Fixed and demineralized hemimandibles were embedded in Tissue-Tek OCT (Sakura, Netherlands) and frozen in liquid nitrogen. 5-µm-thick sections were obtained on an American Optical Cryo-Cut microtome (American Optical, USA) at –20 °C, placed on Superfrost Plus glass slides (Fisher Scientific, USA), and stored at –20 °C. Before use, slides were immersed in two exchanges of water for 2 min each to remove OCT, and then placed in stirred 12.5% EDTA for 24 h to ensure complete demineralization. EDTA was removed by immersion in 2 changes of water for 15 min each.

Remineralization: Mineralizing solutions were prepared according to specifications of Nakamura[26] (for m-SBF) or Beniash and co-workers[15] (for CaP solutions). Ionic compositions of all solutions used are given in Table 1. In some cases, polyaspartic acid (polyAsp) sodium salt, (MW 5–15 kDa, MP Biomedicals, France) was added to m-SBF and CaP solutions at a concentration of 62.5–125 µg/mL.

For TEM, grids were floated on 1 mL of remineralizing solution in an Eppendorf micro centrifuge tube held in a container at 100% humidity and 37 °C. For each time point, grids were removed from the mineralizing solution and washed in two changes of water, and wicked dry. For light microscopy, slides were immersed in gently stirred remineralizing solution within Coplin jars at 37 °C. Slides were removed and washed in 2 changes of water for 5 min each.

Microscopy: Electron microscopy was conducted on unstained ultrathin sections using a Technai 20 TEM (FEI, Hillsboro, OR) with an AMT 1600 side mount camera and LaB6 filament at 200 kV. Energy dispersive X-ray analysis was performed using an EDAX Phoenix system (EDAX, Mahwah, NJ). Ca/P ratios are reported as averages +/- standard deviation.

For light microscopy, thick sections were stained using 1% Alizarin Red at pH 6.1 for 3.5 min. The slides were then differentiated for 30 s in acidified ethanol (95%, 0.05 mL HCl) and dehydrated in 2 changes of 100% ethanol. The sections were cleared in two changes of xylene for 1 min each and mounted in Cytoseal XYL (Richard-Allan Scientific, Kalamazoo, MI). Microscopy was performed on an Olympus BX51 microscope (Olympus, Toronto, ON) with an Infinity 1 camera attachment (Lumenera, Ottawa, ON).

Acknowledgements

We thank Ben Ganss for insightful discussions, and Feryal Sarraf for assistance with cryo-sectioning of thick sections for light microscopy. Electron microscopy was performed at the Advanced Bioimaging Centre (Mount Sinai Hospital, Toronto). This work was supported by a National Sciences and Engineering Research Council of Canada (NSERC) Discovery grant to EDS. We are grateful for NSERC scholarships to AJL (CREATE Program in Regenerative Medicine), BDQ (Post Graduate Scholarship) and JWM (Undergraduate Summer Research Award).

Received: December 18, 2012
Revised: March 22, 2013
Published online: April 19, 2013

[1] S. Weiner, H. D. Wagner, *Annu. Rev. Mater. Sci.* **1998**, *28*, 271.
[2] W. J. Landis, M. J. Song, A. Leith, L. McEwen, B. F. McEwen, *J. Struct. Biol.* **1993**, *110*, 39.
[3] R. A. Robinson, M. L. Watson, *Ann. NY Acad. Sci.* **1955**, *60*, 596.
[4] W. Traub, T. Arad, S. Weiner, *Proc. Natl. Acad. Sci. U.S.A.* **1989**, *86*, 9822.
[5] R. A. Robinson, M. L. Watson, *Anat. Rec.* **1952**, *114*, 383.
[6] E. Beniash, *WIREs Nanomed. Nanobiotechnol.* **2011**, *3*, 47.
[7] A. L. Boskey, *J. Cell. Biochem.* **1998**, 83.
[8] A. George, A. Veis, *Chem. Rev.* **2008**, *108*, 4670.
[9] A. L. Boskey, M. Maresca, S. Doty, B. Sabsay, A. Veis, *Bone Miner.* **1990**, *11*, 55.
[10] W. G. Stetler-Stevenson, A. Veis, *Calcif. Tissue Int.* **1986**, *38*, 135.
[11] J. D. Termine, E. D. Eanes, K. M. Conn, *Calcif. Tissue Int.* **1980**, *31*, 247.
[12] Y. Doi, T. Horiguchi, S. H. Kim, Y. Moriwaki, N. Wakamatsu, M. Adachi, K. Ibaraki, K. Moriyama, S. Sasaki, H. Shimokawa, *Arch. Oral Biol.* **1992**, *37*, 15.
[13] M. J. Olszta, X. Cheng, S. S. Jee, R. Kumar, Y. Y. Kim, M. J. Kaufman, E. P. Douglas, L. B. Gower, *Mater. Sci. Eng. R Rep.* **2007**, *58*, 77.
[14] J. Mahamid, A. Sharir, L. Addadi, S. Weiner, *Proc. Natl. Acad. Sci. U.S.A.* **2008**, *105*, 12748.
[15] A. S. Deshpande, E. Beniash, *Cryst. Growth Des.* **2008**, *8*, 3084.
[16] F. Nudelman, K. Pieterse, A. George, P. H. Bomans, H. Friedrich, L. J. Brylka, P. A. Hilbers, G. de With, N. A. Sommerdijk, *Nat. Mater.* **2010**, *9*, 1004.
[17] Y. Liu, Y. K. Kim, L. Dai, N. Li, S. O. Khan, D. H. Pashley, F. R. Tay, *Biomaterials* **2011**, *32*, 1291.
[18] S. S. Jee, R. K. Kasinath, E. Dimasi, Y. Y. Kim, L. Gower, *CrystEngComm* **2011**, *13*, 2077.
[19] T. T. Thula, F. Svedlund, D. E. Rodriguez, J. Podschun, L. Pendi, L. B. Gower, *Polymers* **2011**, *3*, 10.
[20] Y. Wang, T. Azaïs, M. Robin, A. Vallée, C. Catania, P. Legriel, G. Pehau-Arnaudet, F. Babonneau, M. M. Giraud-Guille, N. Nassif, *Nat. Mater.* **2012**, *11*, 724.
[21] J. W. Freeman, F. H. Silver, *Connect. Tissue Res.* **2005**, *46*, 107.
[22] J. Chen, C. Burger, C. V. Krishnan, B. Chu, B. S. Hsiao, M. J. Glimcher, *Macromol. Chem. Phys.* **2005**, *206*, 43.
[23] P. A. Price, D. Toroian, J. E. Lim, *J. Biol. Chem.* **2009**, *284*, 17092.
[24] T. T. Thula, D. E. Rodriguez, M. H. Lee, L. Pendi, J. Podschun, L. B. Gower, *Acta Biomater.* **2011**, *7*, 3158.
[25] J. Kirkham, S. J. Brookes, R. C. Shore, W. A. Bonass, C. Robinson, *Connect. Tissue Res.* **1995**, *33*, 23.
[26] M. Raspanti, C. Cesari, V. De Pasquale, V. Ottani, R. Strocchi, G. Zucchelli, A. Ruggeri, *Arch. Oral Biol.* **2000**, *45*, 185.
[27] A. Oyane, H. M. Kim, T. Furuya, T. Kokubo, T. Miyazaki, T. Nakamura, *J. Biomed. Mater. Res., Part A* **2003**, *65*, 188.
[28] A. Nanci, *Ten Cate's oral histology: Development, structure, and function*, Mosby, Inc., St. Louis, MO **2007**.
[29] A. L. Boskey, A. S. Posner, *Mat. Res. Bull.* **1974**, *9*, 907.
[30] X. Yang, B. Xie, L. Wang, Y. Qin, Z. J. Henneman, G. H. Nancollas, *CrystEngComm* **2011**, *13*, 1153.
[31] A. J. Hodge, *Connect. Tissue Res.* **1989**, *21*, 137.
[32] M. D. McKee, A. Nanci, W. J. Landis, Y. Gotoh, L. C. Gerstenfeld, M. J. Glimcher, *J. Bone Miner. Res.* **1991**, *6*, 937.
[33] F. Nudelman, P. H. H. Bomans, A. George, G. De With, N. A. J. M. Sommerdijk, *Far. Discussions* **2012**, *159*, 357.
[34] N. C. Blumenthal, A. S. Posner, J. M. Holmes, *Mater. Res. Bull.* **1972**, *7*, 1181.
[35] J. L. Meyer, E. D. Eanes, *Calcif. Tissue Res.* **1978**, *25*, 209.
[36] E. D. Eanes, *Calcif. Tissue Res.* **1977**, *23*, 259.
[37] P. Bar-Yosef Ofir, R. Govrin-Lippman, N. Garti, H. Füredi-Milhofer, *Cryst. Growth Des.* **2004**, *4*, 177.
[38] J. D. Termine, A. S. Posner, *Arch. Biochem. Biophys.* **1970**, *140*, 307.
[39] S. Omelon, J. Georgiou, Z. J. Henneman, L. M. Wise, B. Sukhu, T. Hunt, C. Wynnyckyj, D. Holmyard, R. Bielecki, M. D. Grynpas, *PLoS ONE* **2009**, *4*, e5634.
[40] L. Knott, A. J. Bailey, *Bone* **1998**, *22*, 181.
[41] Y. Kuboki, G. L. Mechanic, *Calcif. Tissue Int.* **1982**, *34*, 306.
[42] A. Veis, *Curr. Opin. Solid State Mater. Sci.* **1997**, *2*, 370.
[43] K. T. Ababneh, R. C. Hall, G. Embery, *Arch. Oral Biol.* **1998**, *43*, 235.
[44] W. T. Butler, J. C. Brunn, C. Qin, M. D. McKee, *Connect. Tissue Res.* **2002**, *43*, 301.
[45] B. A. Gotliv, A. Veis, *Calcif. Tissue Int.* **2007**, *81*, 191.